NASA TECHNICAL NOTE

NASA TN D-2717

EXPERIMENTS ON INDUCTIVE AND CAPACITIVE RADIOFREQUENCY HEATING OF A HYDROGEN PLASMA IN A MAGNETIC FIELD

by Clyde C. Swett

Lewis Research Center

Cleveland, Ohio

NATIONAL AERONAUTICS AND SPACE ADMINISTRATION • WASHINGTON, D. C. • MARCH 1965

NASA TN D-2717

EXPERIMENTS ON INDUCTIVE AND CAPACITIVE RADIOFREQUENCY HEATING OF A HYDROGEN PLASMA IN A MAGNETIC FIELD

By Clyde C. Swett

Lewis Research Center
Cleveland, Ohio

NATIONAL AERONAUTICS AND SPACE ADMINISTRATION

For sale by the Office of Technical Services, Department of Commerce,
Washington, D.C. 20230 -- Price $1.00

EXPERIMENTS ON INDUCTIVE AND CAPACITIVE RADIOFREQUENCY HEATING OF A HYDROGEN PLASMA IN A MAGNETIC FIELD*

by Clyde C. Swett

Lewis Research Center

17880

SUMMARY

Experimental results for heating a plasma by a radiofrequency (rf) coil having an ungrounded electrostatic shield are analyzed by using an electric-circuit model based mainly on the geometric character of the apparatus. This model indicates that the presence of a plasma adds a "lossy" capacitor in parallel with the rf coil. Consequently, power goes into the plasma both inductively (E_θ) and electrostatically (E_r,E_z). It is believed that the electrostatic mode of power transfer is responsible for some anomalies noted in plasma experiments. The amount of power in each mode was calculated and shown to vary with magnetic field. The inductive power transfer increased at magnetic-field values near the atomic and molecular ion cyclotron fields, whereas the electrostatic power decreased or increased depending on which parameter - power or coil voltage - was held constant. Maximum total power transfer was as high as 90 percent of the input power and occurred near the atomic and molecular ion cyclotron resonance fields. The electron-density decrease noted near the resonant points appeared to be related to the induction mode only. Some deficiencies of this simple model are noted, and the importance of accurate measurements in this type of analysis is indicated.

Author

INTRODUCTION

One of the problems that exists in the plasma physics field is that of obtaining, in the laboratory, experimental conditions that approximate those assumed in theoretical analyses. For example, in the field of radiofrequency (rf coil-generated plasma waves, discrepancies between calculated and experimental results have been noted in wavelengths, in the amplitudes of wave compoments, in the absence of theoretical resonances, and in the shifts in resonant frequency toward low magnetic fields rather than toward high magnetic fields. These discrepancies are undoubtedly due to deficiencies in the experimental setup.

---

*An abbreviated version of this report was presented at the American Physical Society, Division of Plasma Physics Meeting, San Diego, California, November 6-9, 1963.

As part of an rf plasma heating program at the Lewis Research Center, studies are being made of one experimental factor that may be partly responsible for the anomalies. This factor is the rf coil itself. Such a coil not only generates azimuthal electric fields but also radial and axial fields. Under certain conditions, axial electrical fields may even exist in portions of the plasma not directly under the coil. Hence, the coil is not a simple source for transferring power to a plasma. A study of how the power is transferred from the coil to the plasma by the various electric fields should indicate whether or not the coil could account for the anomalies noted. To a certain extent these fields can be controlled or altered by shields near the coil.

The simplest coil configuration that can be visualized is that in which a grounded electrostatic shield is installed between the coil and plasma. For such a configuration, only one electric field is generated - an azimuthal electric field. Experimental results that utilize this configuration are reported in reference 1. In other related studies, the shield was not used (refs. 2 to 6).

Another possible configuration is that in which the electrostatic shield is present but ungrounded. This more complicated arrangement should result in azimuthal and radial electric fields directly underneath the shield but should eliminate the axial field directly underneath the coil. Axial fields may, however, be present in the plasma between the ends of the shield and grounded portions of the system. The axial and radial fields result from an rf voltage existing on the shield due to capacitive coupling between the coil and the shield.

The present experimental program was undertaken to determine how much the power transfer could be improved by using the ungrounded electrostatic-shield configuration, since it was believed that the resulting fields would be strong and would enhance power transfer. Also, it was desired to determine if the total power could be analytically separated into two different heating modes - the induction heating mode normally associated with coils, and the capacitive or electrostatic heating mode that results from capacitive coupling between coil and shield. The most promising method for accomplishing this appeared to be by determination of an equivalent electric-circuit model of the coil-shield combination that could be used with experimental data to calculate the power distribution.

SYMBOLS

a_n coefficients of terms in eq. (2)

b_n coefficients of terms in eq. (3)

C capacitance between coil and shield, F

C_1 capacitance of equivalent network, F

E peak coil voltage, V

E_r electric field in r-direction

E_s peak a-c voltage on shield

E_z electric field in z-direction

E_θ electric field in θ-direction

f generator frequency, mc

f_m frequency, k mc

I network current, amp

j complex operator

L coil inductance, 3.46×10^{-6} H

$\mathfrak{L}$ inductance of equivalent circuit, H

l path length through plasma, cm

n_e electron density, electrons/cc

P power from rf source, W

P_C power dissipated in capacitive branch of circuit, W

P_L power dissipated in inductive branch of circuit, $P_R + P_p$, W

P_R power dissipated in coil resistance, W

P_p power dissipated by induction heating in plasma, W

P_t total power in microwave interferometer, mW

P_1 power in reference arm of microwave interferometer, mW

P_2 power in plasma arm of microwave interferometer, mW

R a-c coil resistance, ohms

R_C resistance of capacitive branch, ohms

R_L resistance of inductive branch, $R + R_p$, ohms

R_p resistance in inductive branch caused by plasma, ohms

$\mathfrak{R}$ resistance of equivalent circuit, ohms

θ phase angle, deg

$\Delta\theta$ phase angle change, deg

ω angular frequency, $2\pi f$, $2\pi 6.5 \times 10^6$ rad/sec

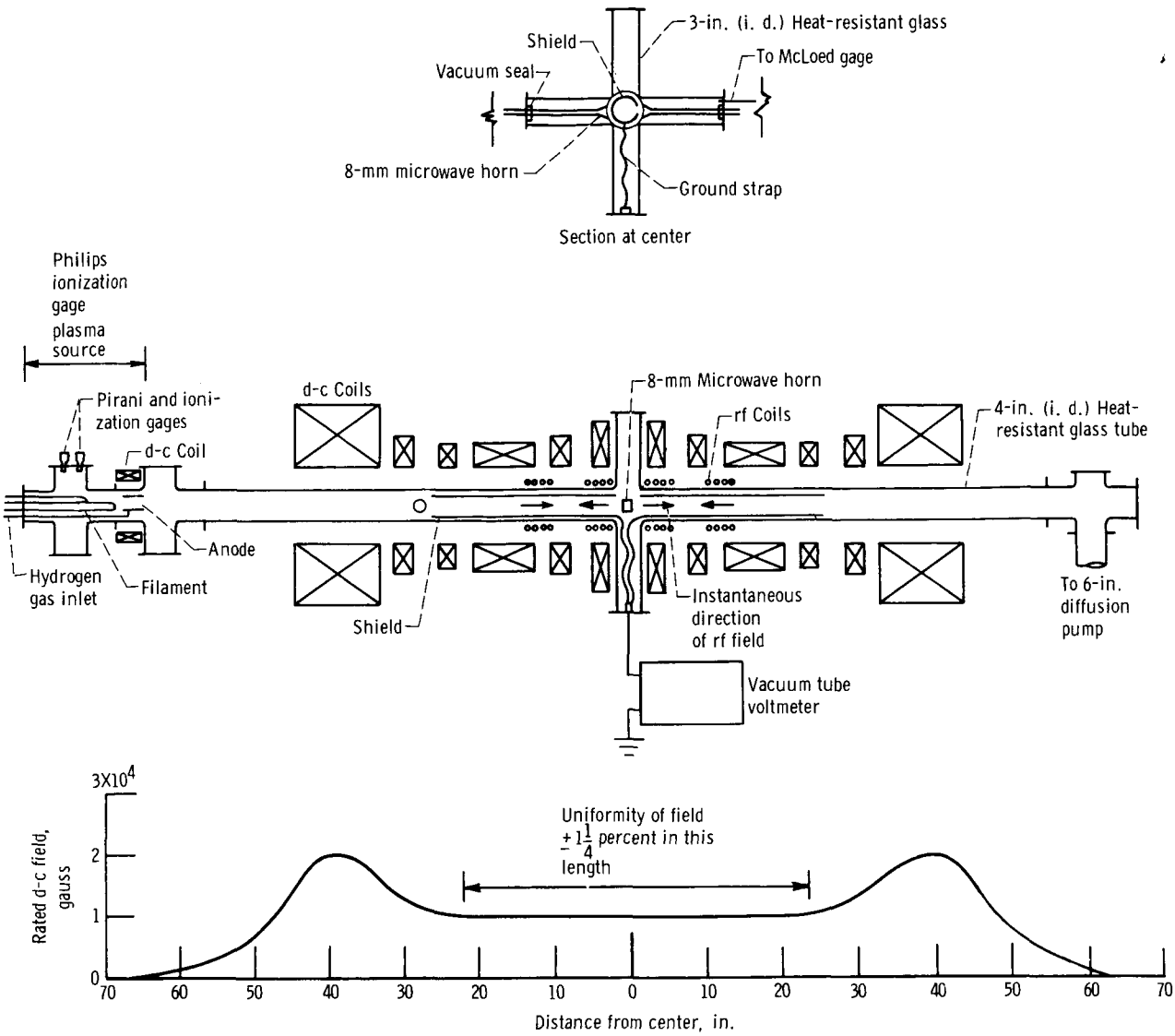

Figure 1. - Configuration of ion cyclotron resonance apparatus 2 (ICRA 2).

BASIC EXPERIMENTAL CONFIGURATION

The actual apparatus for which an electric-circuit model is to be developed is shown in figure 1. A basic representation of this apparatus is shown in figure 2(a), in which only the left half is shown; the right half is identical except for elimination of the plasma source. A glass tube is located in a steady axial magnetic field and has a plasma column along the axis. An rf coil is wrapped around the tube. Inside of the glass tube is an electrostatic shield split longitudinally so that an azimuthal electric field can be generated inside of the shield.

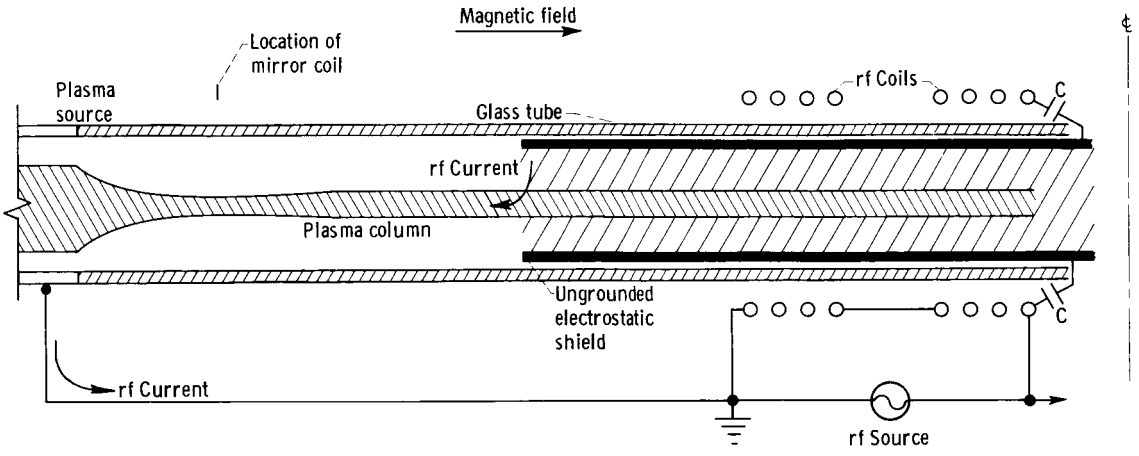

(a) Basic experimental configuration.

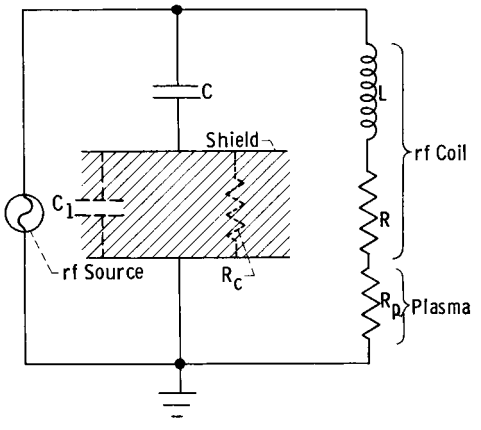

(b) Electric-circuit model including capacitance of equivalent network.

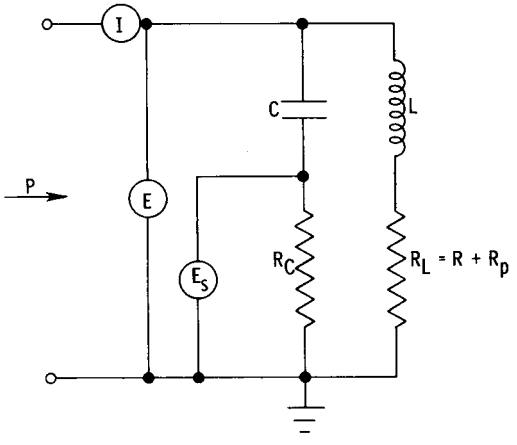

(c) Electric-circuit model where capacitance of equivalent network is zero.

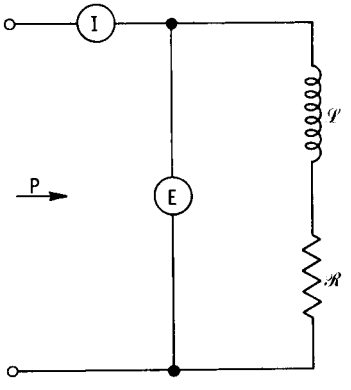

(d) Circuit equivalent of electric-circuit model where capacitance of equivalent network is zero (part (c)).

Figure 2. - Basic experimental configuration and circuit models.

In figure 2(b) the rf coil has been represented as an inductance L in series with the a-c resistance R of the coil. These quantities L and R would be measured at the terminals of the coil without plasma present; that is, the effects of distributed capacitance are already included in them. When plasma is present there is an additional resistance R_p that represents the additional induction heating load due to the plasma, the greater the load the larger the value of R_p. The shield is located such that there can be capacitive coupling between coil and shield. For simplicity, this capacitance, although it is actually a distributed quantity, has been assumed to have an equivalent value C between the high-voltage terminal of the coil and shield (figs. 2(a) and (b)). Because the coupling results in a voltage on the shield, there is a radial electric field between the shield and the plasma column and an axial electric field between the shield and ground so that current can flow from the coil to the shield and to ground through the plasma.

Between the shield and ground there is a complicated series and parallel network of capacitances, inductances, and resistances. For example, there is capacitance between the shield and plasma column and between the shield and external structures, resistance in the weak plasma lying between the shield and the plasma column, resistance in the plasma column between the shields and the ends of the tube, and inductances in the plasma column and ground-return paths. The network, however, can be reduced to an equivalent parallel network consisting of a capacitance C_1 in parallel with a resistance R_C (fig. 2(b)). For the present program the capacitance C_1 has been assumed to be negligible. The circuit model then is as shown in figure 2(c), where R and R_p have been combined into R_L, which is the resistance in the inductive branch. The capacitive branch consists of C and R_C, which can be considered as a "lossy" condenser in parallel with the coil. The peak a-c voltage on the shield is E_s, the peak coil voltage is E, the root-mean-square current through the network is I, and the power dissipated in the network is P. This four-element circuit can be readily transformed to an equivalent two-element series circuit consisting of an inductance $\mathfrak{L}$ and resistance $\mathfrak{R}$ as shown in figure 2(d).

CIRCUIT ANALYSIS

The circuits to be analyzed are those shown in figures 2(c) and (d). The assumptions are that L is known and constant, that C_1 can be neglected, that $(\omega L)^2 \gg (R_L)^2$, and that $(\omega \mathfrak{L})^2 \gg (\mathfrak{R})^2$. The unknowns are C, R_C, and R_L, requiring that three simultaneous equations must be solved.

The first equation relates the power input P to the power dissipated in the two resistive elements R_L and R_C:

$$P = P_L + P_C = \frac{E_s^2}{2R_C} + \frac{E^2 R_L}{2\left[R_L^2 + (\omega L)^2\right]}$$

With the assumption that $(\omega L)^2 \gg R_L^2$,

$$P = \frac{E_s^2}{2R_C} + \frac{E^2 R_L}{2\omega^2 L^2} \tag{1}$$

The number 2 enters in converting peak voltages to root-mean-square voltages.

The second equation relates voltage and current to the absolute impedance of the equivalent circuit (fig. 2(d)):

$$\frac{E}{\sqrt{2}\ I} = \left|\mathcal{R} + j\omega\mathcal{L}\right| = \sqrt{\mathcal{R}^2 + (\omega\mathcal{L})^2}$$

With the assumption that $(\omega\mathcal{L})^2 \gg (\mathcal{R})^2$,

$$\frac{E}{\sqrt{2}\ I} = \omega\mathcal{L} \tag{2}$$

The third equation relates the power input to the current and resistance of the equivalent circuit:

$$P = I^2\mathcal{R} \tag{3}$$

It can easily be shown from equivalent-circuit theory that

$$\mathcal{R} = \frac{\omega^2 C^2 R_C R_L (R_C + R_L) + \omega^4 C^2 R_C L^2 + R_L}{\omega^2 C^2 (R_C + R_L)^2 + (1 - \omega^2 LC)^2}$$

and

$$\omega\mathcal{L} = \frac{\omega^3 R_C^2 C^2 L - \omega C R_L^2 - \omega^3 L^2 C + \omega L}{\omega^2 C^2 (R_C + R_L)^2 + (1 - \omega^2 LC)^2}$$

The procedure used to solve the equations is as follows: First, equation (1) was solved for R_L, and then R_L was substituted in equations (2) and (3) leaving two equations in the two unknowns R_C and C. Then the resulting equations were solved simultaneously on an IBM 7090 computer for R_C and C. With R_C known, R_L, P_L, and P_C could be determined. Then the power P_R dissipated in the resistance of the coil could be calculated from $P_R = (R/R_L)P_L$.

Equation (2), on substitution of R_L, reduces to the form,

$$a_1 C^2 R_C^2 + a_2 C^2 R_C + a_3 C^2 + a_4 C^2 R_C^3 + a_5 R_C^2 + a_6 C R_C^2 + a_7 C^2 R_C^4 + a_8 C R_C + a_9 C = 0$$

where

$$a_1 = \frac{4P^2\omega^6L^4}{\sqrt{2}\ IE^3} - \frac{2\omega^4L^2E_s^2}{\sqrt{2}\ EI} + \frac{E\omega^4L^2}{\sqrt{2}\ I}$$

$$a_2 = -\frac{4\omega^6L^4PE_s^2}{\sqrt{2}\ IE^3}$$

$$a_3 = \frac{E_s^4\omega^6L^4}{\sqrt{2}\ IE^3}$$

$$a_4 = \frac{4\omega^4L^2P}{\sqrt{2}\ IE}$$

$$a_5 = \frac{E}{\sqrt{2}\ I} - \omega L$$

$$a_6 = -\frac{2E\omega^2L}{\sqrt{2}\ I} + \frac{4\omega^5L^4P^2}{E^4} + \omega^3L^2$$

$$a_7 = \frac{E\omega^2}{\sqrt{2}\ I} - \omega^3L$$

$$a_8 = \frac{-4\omega^5L^4PE_s^2}{E^4}$$

and

$$a_9 = \frac{E_s^4\omega^5L^4}{E^4}$$

Equation (3), on substitution of R_L, reduces to the form

$$b_1C^2R_C^2 + b_2C^2R_L + b_3C^2 + b_4C^2R_C^3 + b_5C^2R_C^4 + b_6R_C^2 + b_7CR_C^2 + b_8R_C = 0$$

where

$$b_1 = \frac{4P^3\omega^6L^4}{E^4I^2} - \frac{2PE_s^2\omega^4L^2}{I^2E^2} + \frac{P\omega^4L^2}{I^2} + \frac{4PE_s^2\omega^6L^4}{E^4}$$

$$b_2 = -\frac{4P^2E_s^2\omega^6L^4}{I^2E^4} - \frac{E_s^4\omega^6L^4}{E^4}$$

$$b_3 = \frac{PE_s^4\omega^6L^4}{I^2E^4}$$

$$b_4 = \frac{4P^2\omega^4L^2}{I^2E^2} - \frac{4P^2\omega^6L^4}{E^4} + \frac{E_s^2\omega^4L^2}{E^2} - \omega^4L^2$$

$$b_5 = \frac{P\omega^2}{I^2} - \frac{2\omega^4L^2P}{E^2}$$

$$b_6 = \frac{P}{I^2} - \frac{2\omega^2L^2P}{E^2}$$

$$b_7 = -\frac{2P\omega^2L}{I^2}$$

and

$$b_8 = \frac{E_s^2\omega^2L^2}{E^2}$$

These equations were used to compare the data taken in this investigation. The following parameters were constant:

$$\omega = 2\pi 6.5\times10^6 \text{ rad/sec}$$

$$L = 3.46\times10^{-6} \text{ H}$$

$$R = 0.55 \text{ ohm}$$

EXPERIMENTAL APPARATUS

A longitudinal cross section of the ion-cyclotron-resonance apparatus (ICRA 2) used for this program is shown in figure 1 (p. 4). Ultrapure hydrogen was introduced into the Philips-ionization-gage-type discharge and pumped out at the other end of the system by a 6-inch diffusion pump. The base pressure of the system was about 10^{-7} torr. The operating pressure (2.0μ) was controlled by the amount of gas flow and was measured at the center of the apparatus by a McLeod gage that has a liquid-nitrogen cold trap. The 4-inch inside-diameter heat-resistant glass discharge tube had 3-inch inside-diameter arms in the center for the microwave horns, for connections to the shield, and for

connections to the McLeod gage. Twelve water-cooled d-c coils connected in series and supplied with up to 4400 amperes from remotely controlled generators produced a maximum field of 10,000 gauss in the region of the rf coil and 20,000 gauss in the mirrors. The field variation was $\pm 1\frac{1}{4}$ percent in the uniform region as measured by a nuclear-magnetic-resonance gaussmeter.

The rf coil was a four-section coil with four turns per section. It was fabricated by using 3/8-inch copper tubing coated with either polyethylene insulation or a baked-epoxy tape. The coils were connected as shown in reference 2 to give the instantaneous magnetic-field directions shown in figure 1 (p. 4). The wavelength - distance between the center of the first coil and the center of the third coil - was 16 inches, and the inside diameter of the coil was $5\frac{3}{8}$ inches. The inductance of the coil was 3.46×10^{-6} henry, and the a-c resistance of the coil was 0.55 ohm, as measured by an impedance bridge. The coil was cooled with warm water (115° F) to prevent water vapor in the room from condensing and dripping down onto the matching network terminals.

The electrostatic shield under the rf coil was rolled from 1/16-inch sheet aluminum in two sections, each section having a longitudinal slot. Each section was 36 inches long and connected to a flange in the bottom arm of the glass tube by means of flexible copper straps. It was necessary to install this shield inside of the glass tube because of arcing problems between the shield and coil when it was located outside of the tube. The a-c voltage on the shield was measured by a vacuum-tube voltmeter.

The output impedance of the transmitter was matched to the coil in two stages - a 600- to 50-ohm balun and then a 50-ohm L-pad matching network. A directional coupler was used to measure both the power output and any reflected power due to mismatch. In normal operation the matching network was carefully adjusted so that the reflected power was always less than 10 watts. The rated power output of the transmitter is 15 kilowatts continuous operation and the frequency range is 4 to 28 megacycles. For this program a maximum power of 3100 watts was used at a frequency of 6.5 megacycles.

Electron densities were measured by means of an 8-millimeter microwave interferometer diagramed in figure 3. The amplitude of the signals in the reference arm and the plasma arm were determined separately, and then the combined signal was measured both with and without plasma. The phase difference between the signals in the reference arm and the plasma arm was then computed by using the relation (ref. 7):

$$\cos \theta = \frac{\frac{P_t}{P_1} - \left(1 + \frac{P_2}{P_1}\right)}{2\sqrt{\frac{P_2}{P_1}}}$$

for both plasma and no-plasma conditions. The electron density was calculated

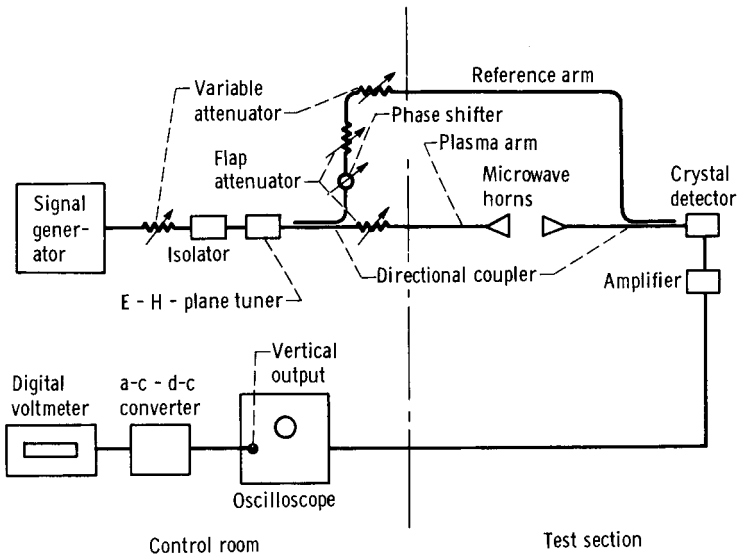

Figure 3. - Schematic diagram of microwave interferometer.

from the phase change

$$n_e = 2.07 \times 10^9 \left(\frac{\Delta\theta}{l}\right) f_m$$

Further discussion of this type of system is given in reference 7.

RESULTS AND DISCUSSION

A typical set of data obtained in the apparatus and to be used with the analysis is shown in figures 4 and 5 (p. 12). Generally, data have been obtained as a function of axial magnetic field for two different modes of operation: (1) where the power output P of the rf source is held constant and (2) where the coil voltage E is held constant. Besides the parameters P and E, the variation of the network current I, the a-c voltage of the shield E_s, and the electron density n_e are also shown.

The curves indicate by either increase in power for the constant-voltage runs or decrease in voltage for the constant-power runs that power absorption is greater at magnetic fields equal to or slightly less than the atomic and molecular hydrogen-ion resonant-field values indicated. Peaks or valleys are also noted in the other parameters at or near these power-absorption peaks. Further increase in power or coil voltage results in a slight, but definite, shift of the maximum absorption toward lower fields.

Probably the most important curve in the sense that it prompted the present work is the network-current variation (fig. 5(c)). If the rf coil could be represented simply as an inductance in series with a resistance as is usually done, then, with constant voltage, the current should remain constant. (Usually the inductive reactance is so large compared with the resistance, even when plasma loading is present, that the reactance will be the factor which

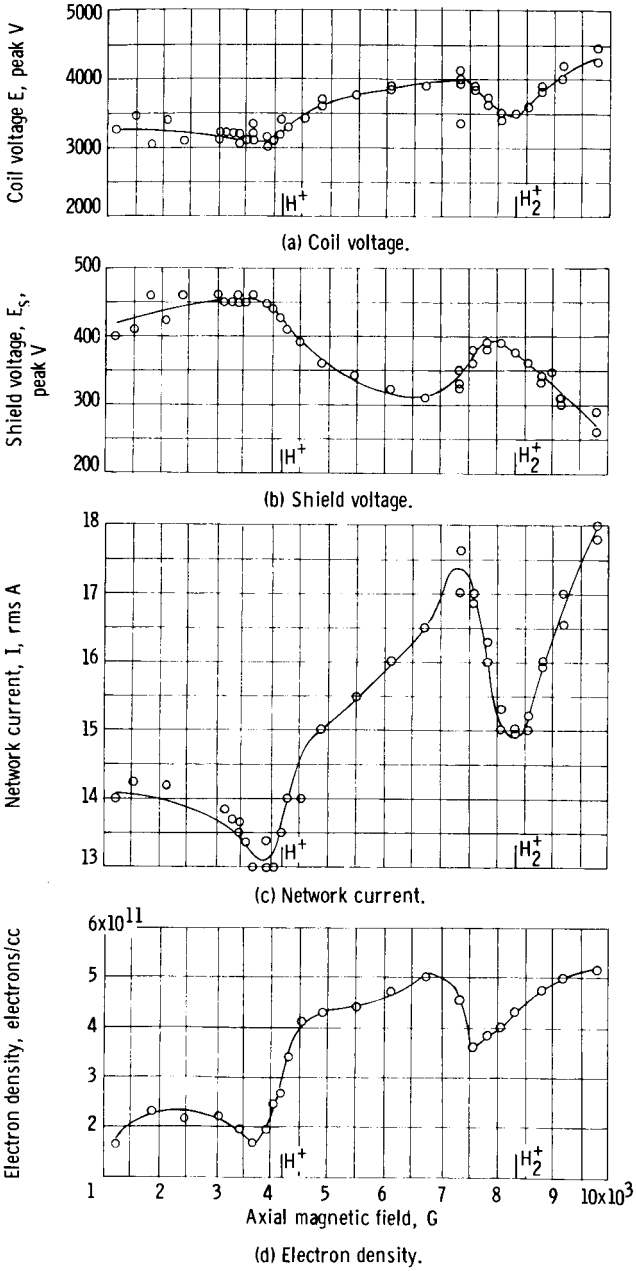

Figure 4. - Typical experimental data. Constant rf power, 1800 watts.

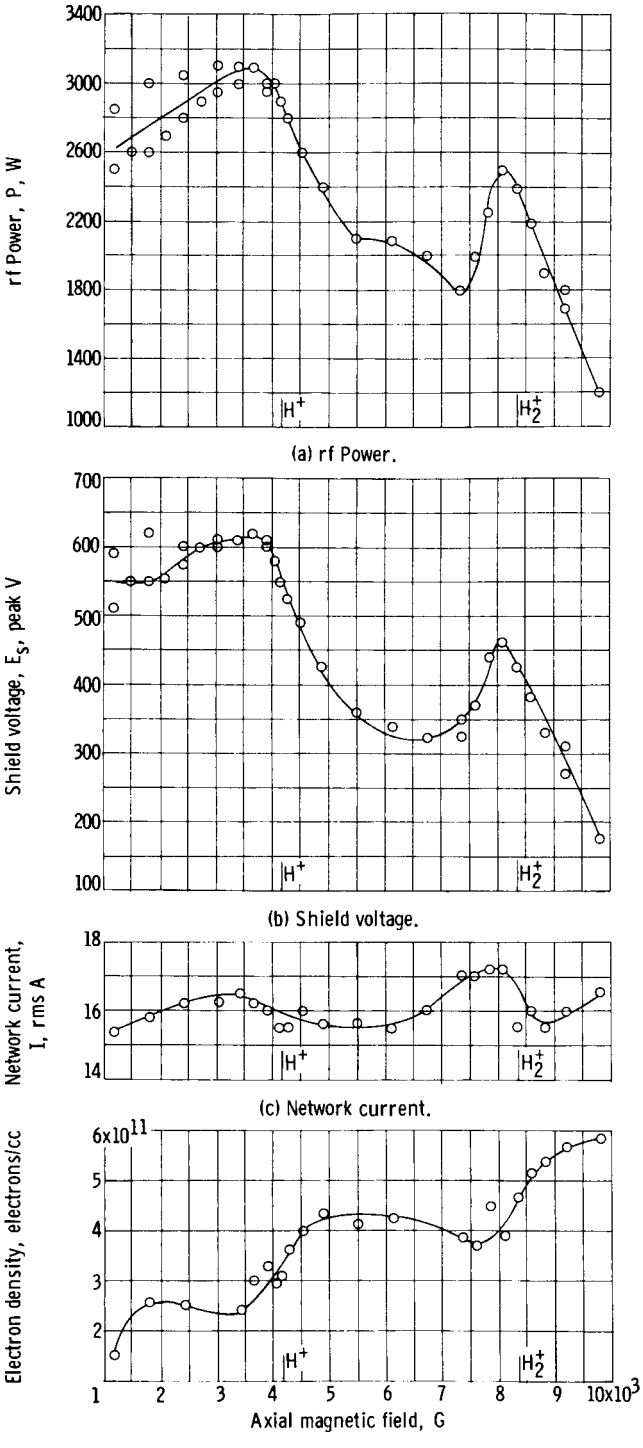

Figure 5. - Typical experimental data. Constant coil voltage, 4000 volts.

determines the current through the coil; consequently, the current should be constant if the reactance is constant). Since the current is not constant, the coil cannot be represented as a simple two-element network. This report considers it is possible to represent the rf coil more closely as a four-element network. The exact network is undoubtedly more complicated than this.

A comparison of the power transfer for the ungrounded-shield configuration and the grounded-shield configuration (ref. 1) is shown in the following table:

Shield configuration	rf power, W	Peak coil voltage, V
Ungrounded	1800	3190
Grounded	730	5500

It is apparent that the power transfer has been improved even without considering the difference in voltage. The power for the ungrounded-shield configuration would have been considerably larger if the coil voltage had been run at 5500 volts. However, consideration must be given to the facts that different plasma heating modes may be present, that efficiencies of power transfer are undoubtedly different, and that electron densities for the configurations are not identical.

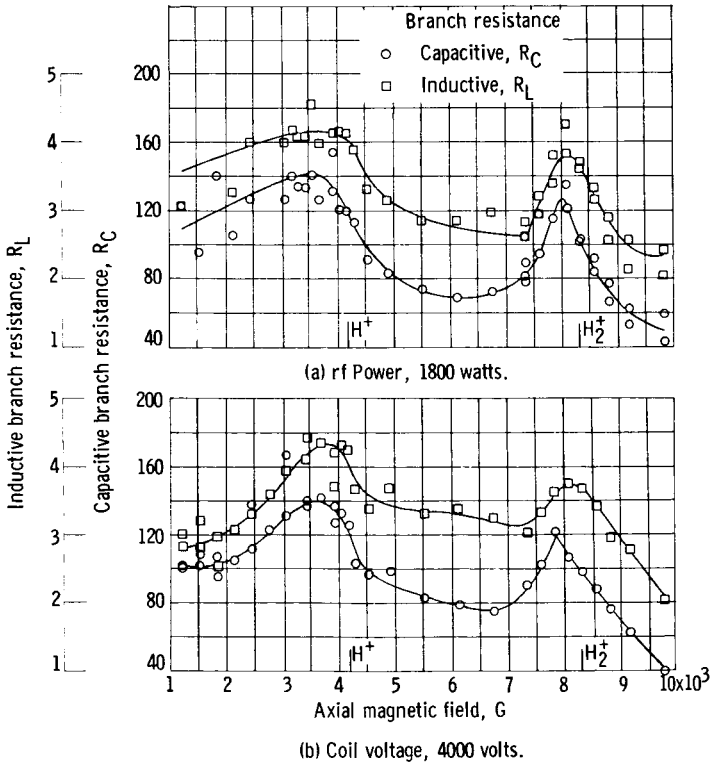

Figure 6. - Effect of axial magnetic field on capacitive and inductive branch resistance.

The quantities R_C, R_L, and C were determined by using data such as these in simultaneous equations. Calculations were also made to show that the approximations used were valid. For a typical point $(\omega\mathfrak{L}/\mathfrak{R})^2 = 760$, while $(\omega L/R_L)^2 = 1550$.

Figure 6 shows the effect of magnetic field on R_C and R_L for the two operating modes. The operating mode does not have much effect on how the resistances vary. Originally it was thought that the peaks and/or valleys for R_C and R_L would occur at different magnetic fields, indicating the presence of at least two separate and distinct phenomena. One of the phenomena would be the induction or azimuthal heating of the ions; the other would primarily be the heating of electrons as a result of the capacitive coupling. The former heating mode which is of primary

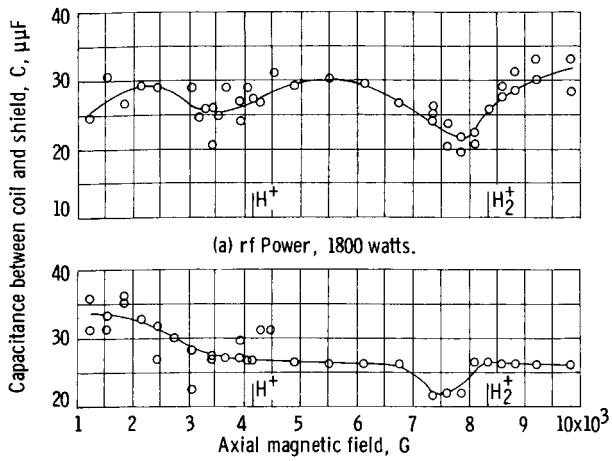

Figure 7. - Effect of axial magnetic field on capacitance.

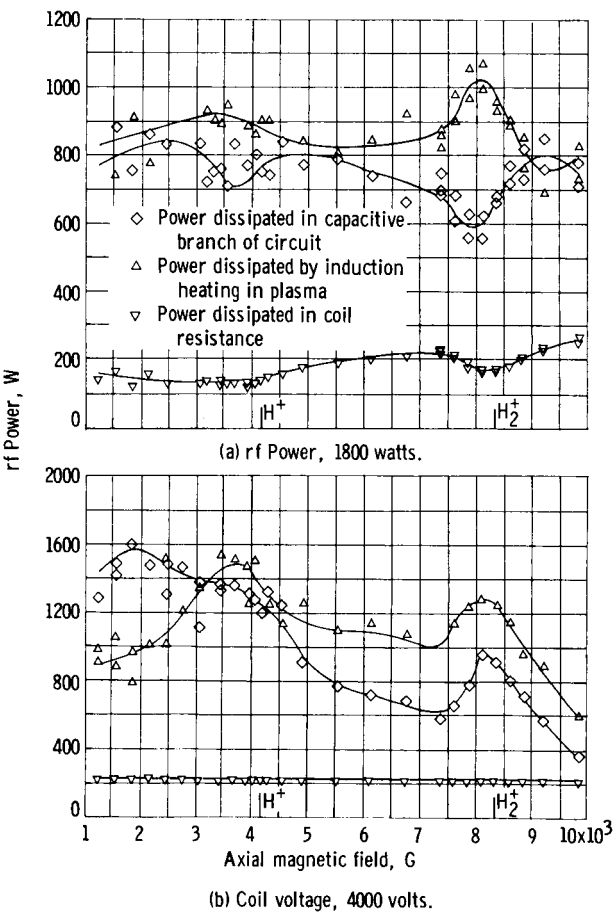

Figure 8. - Distribution of rf power among power dissipated in capacitive branch of circuit, by induction heating in plasma, and in coil resistance.

interest would manifest itself by a resonance occurring either at the atomic and molecular resonant fields or at slightly greater fields if ion cyclotron waves were being generated. Since the density used herein is relatively low, ion wave production is unimportant, and R_L should reach a peak at the resonant-field values. Because of the experimental error, it is not definite that this does happen, especially at low magnetic fields where data scatter is great. At high fields there appears to be some separation of the peaks and R_L peaks close to the molecular resonance.

Figure 7 shows how capacitance C varies with magnetic field for both constant-power and constant-voltage runs. Most of the data lie between 25 to 30 micromicrofarads; however, there is a definite indication (especially for the constant-power runs) that C is not constant. If C had remained constant, the assumption that C_1 could be neglected would be justified. If C_1 is not negligible, a slight variation of net capacitance, such as that observed, would occur in the lossy branch of the circuit, because the series resultant of a constant capacitance C_1 in parallel with a variable resistance R_C is a variable capacitance in series with a variable resistance. A completely new circuit analysis is needed to determine the exact importance of C_1; however, initial estimates show inclusion to have a minor effect on relative power distribution, which is of primary concern herein.

The distribution of rf power among R, R_p, and R_C is shown in figure 8, and differences are noted depending on whether constant-power data or constant-voltage data are being considered. In the constant-power data (fig. 8(a)) the induction power P_L shows peak power transfer near the resonant points, while the electrostatic power P_C shows de-

creases at these points. This is expected, since power absorption by the ions from induction leaves less power available for the electrostatic mode when the total rf power is constant.

Power divides somewhat differently for the constant-voltage data (fig. 8(b)). In this case, both the induction and electrostatic modes exhibit peaks, but there may be a shift toward lower fields for the electrostatic mode.

Because of the errors involved, as discussed subsequently, only two general statements should be made on the power-distribution results: Power divides about equally between the induction and electrostatic modes, and the efficiency of the total power transfer from the coil to the plasma $[(P - P_R)/P]100$ approaches 90 percent. This efficiency of 90 percent represents an improvement over the 60-percent efficiency quoted in reference 1. Whether such improvement is important is questionable, however, since it is the result of electrostatic heating that primarily heats electrons rather than ions.

It is somewhat informative to try to correlate the dips noted in the electron density (figs. 4(d) and 5(d), p. 12) with the power distribution (fig. 8) at a field of 7620 gauss, which is near the molecular resonance. (Because of data scatter at the atomic resonant point, a similar correlation at that point is more ambiguous.) It can be seen that the decrease in electron density correlates quite well with the increase of power in the induction mode when both the constant-power and constant-voltage data are considered. The density and induction-power trends are similar for the two sets of data. Hence, it can be concluded that, when power is absorbed by the ions from the azimuthal field, the ion density is reduced.

A calculation was made of the effect of measurement uncertainties (estimated) on the values of R_C, R_L, and C (see table I). These data show that errors in calculated parameters can be considerably larger than the initial measurement errors. It is expected that greater errors will be encountered in more involved circuit configurations, because the exponents of the terms of the simultaneous equations will be larger. Because of the uncertainties involved in this program, trends should be given greater importance than the quantitative results.

TABLE I. - EFFECT OF MEASUREMENT UNCERTAINTIES ON CALCULATED PARAMETERS

Experimental parameter	Uncertainty, percent	Variation in calculated parameter, percent		
		Resistance of inductive branch, R_L	Resistance of capacitive branch, R_C	Capacitance between coil and shield, C
Power dissipated in network, P	5.6	8.6	<1	<1
Coil voltage, E	2.7	15.7	16.5	1.6
Network current, I	6.3	22.3	28.5	39.9
Voltage (a-c) on shield, E_S	2.8	1.5	2.7	<1
Coil inductance, L	4.0	23.8	23.6	31.0

Since the shielded configuration used here is unusual, the relation between this work and that reported for unshielded configurations should be discussed. In some respects the two configurations are similar. Both produce radial electric fields. These fields are stronger with the unshielded coil; however, the length of the region over which this field exists will be much shorter, because the coil is much shorter than the shield. Axial electric fields also exist in both configurations, the unshielded coil having strong fields near the coil and the shielded coil having strong fields off the ends of the shield. Experimentally, it has been observed that it is about equally easy to get the power into the plasma for the two configurations. Also, the unshielded coil has the same anomaly that the current does not remain constant when coil voltage is maintained constant. The unshielded coil should, therefore, also be investigated in terms of equivalent circuitry.

SUMMARY AND CONCLUDING REMARKS

A simple electrical model of an induction coil heating a plasma in a magnetic field has been developed mainly from the geometric character of the apparatus. The model shows that the plasma in effect adds a "lossy" capacitor in parallel with the coil. Considerable power is absorbed by this capacitor and may be responsible for observed anomalies noted in some plasma experiments. The powers transferred in the electrostatic and induction modes have been determined and are shown to vary with magnetic field. A decrease in electron density (or ion density) near the resonant points appeared to be related to the increase in power in the induction mode. Power-transfer efficiency as high as 90 percent was attained. Errors in experimental measurements caused variations in the calculated parameters of up to about eight times the original errors.

Further refinement of the type of analysis described herein may offer a means of describing the conditions more logically that exist under the coil. The analysis especially needs to be broadened to include the more commonly used unshielded rf coils.

Lewis Research Center,
National Aeronautics and Space Administration,
Cleveland, Ohio, December 8, 1964.

REFERENCES

1. Swett, C. C., and Krawec, R.: Preliminary Observations of R. F. Power Transfer to a Hydrogen Plasma at Frequencies near the Ion Cyclotron Frequency. Engineering Aspects of Magnetohydrodynamics, N. W. Mather and G. W. Sutton, eds., Gordon & Breach Pub., 1964, pp. 599-614.

2. Stix, T. H., and Palladino, R. W.: Ion Cyclotron Resonance. Second United Nations Int. Conf. on Peaceful Uses of Atomic Energy, vol. 31, 1958, pp. 282-287.

3. Hooke, W. M., et al.: Experiments on Ion Cyclotron Waves. Phys. of Fluids, vol. 4, no. 9, Sept. 1961, pp. 1131-1141.

4. Stix, T. H., and Palladino, R. W.: Experiments on Ion Cyclotron Resonance. Phys. of Fluids, vol. 1, no. 5, Sept.-Oct. 1958, pp. 446-451.

5. Dubovoi, L. V., Shvets, O. M., and Ovchinnikov, S. S.: Ion Cyclotron Resonance in Dense Plasmas. Plasma Physics (Jour. of Nuclear Energy), pt. C, vol. 3, no. 3, July 1961, pp. 203-208.

6. Sinel'nikov, K. D., et al.: The Investigation of Ion Cyclotron Resonance in Dense Plasma. Soviet Phys.-Tech. Phys., vol. 5, no. 3, Sept. 1960, pp. 261-265.

7. Kuhns, Perry: Microwave Interferometer Measurements of Electron-Ion Recombination in Nitrogen, Air, and Argon. NASA TN D-1191, 1962.